

# Weak Collocation Regression method: fast reveal hidden stochastic dynamics from high-dimensional aggregate data

Liwei Lu<sup>1</sup>, Zhijun Zeng<sup>2</sup>, Yan Jiang<sup>3</sup>, Yi Zhu<sup>4</sup>, and Pipi Hu<sup>\*5</sup>

<sup>1,2,3,4,5</sup>Yau Mathematical Sciences Center, Tsinghua University, Beijing, 100084, China.

<sup>4,5</sup>Yanqi Lake Beijing Institute of Mathematical Sciences and Applications, Beijing, 101408, China

September 7, 2022

## Abstract

Revealing hidden dynamics from the stochastic data is a challenging problem as randomness takes part in the evolution of the data. The problem becomes exceedingly complex when the trajectories of the stochastic data are absent in many scenarios. Here we present an approach to effectively modeling the dynamics of the stochastic data without trajectories based on the weak form of the Fokker-Planck (FP) equation, which governs the evolution of the density function in the Brownian process. Taking the collocations of Gaussian functions as the test functions in the weak form of the FP equation, we transfer the derivatives to the Gaussian functions and thus approximate the weak form by the expectational sum of the data. With a dictionary representation of the unknown terms, a linear system is built and then solved by the regression, revealing the unknown dynamics of the data. Hence, we name the method with the Weak Collocation Regression (WCR) method for its three key components: weak form, collocation of Gaussian kernels, and regression. The numerical experiments show that our method is flexible and fast, which reveals the dynamics within seconds in multi-dimensional problems and can be easily extended to high-dimensional data such as 20 dimensions. WCR can also correctly identify the hidden dynamics of the complex tasks with variable-dependent diffusion and coupled drift, and the performance is robust, achieving high accuracy in the case with noise added.

**Keywords**— stochastic dynamics, the weak form, collocation of kernels, Fokker-Planck equation, aggregate data, revealing hidden dynamics

## 1 Introduction

Nowadays, a large amount of data has been collected in different realms, and revealing the hidden dynamics buried in the data is an essential topic in science and engineering. Such dynamics can be described mathematically through differential equations. In this regard, differential equations derived from the so-called first principle successfully describe nature's phenomena during the past several centuries. The examples include the Navier-Stokes equation in hydrodynamics for fluid

---

\*Corresponding author, hpp1681@gmail.com

dynamics [1], Schrödinger equation in quantum mechanics for probability current [2], Black-Scholes in computational finance for option pricing [3]. Often, the data we collect is a tremendous amount of time series dataset, which accurately describes stochastic differential equations. For instance, Brownian motion for molecular dynamics and geometric Brownian motion for the financial market [4]. On the other hand, leveraging explosive growth of available data, machine learning, especially deep learning, has recently attained tremendous success in computer vision, natural language processing, and many other topics in computer science [5].

Benefiting from these two, plenty of work spring up, and within them, one most important focus is pouring new structures onto modeling the hidden dynamics from data. The physical informed neural network (PINN) adds physical constraints to the data by adding the residual of the differential equations to the loss and making learning coefficients of the unknown terms of the governing equations reliable [6]. Kutz *et al.* proposed a framework named “SINDy” by combining regression and sparse identification to reveal nonlinear dynamical systems [7]. The time-series data always contain many missing points and flaws with the high noise, making analysis hard and tricky. Hu *et al.* proposed using symbolic ODE (ordinary differential equations) to reveal hidden dynamics from time series data [8] with the integration form, making the learning process more stable. More related works about inferring differential equations, see [9, 10, 11, 12, 13, 14, 15]. However, in a more general scenario, the data come from the stochastic process where the determined-dynamic system is not feasible because of the randomness. Revealing hidden dynamics from the stochastic data calls for new structures suited to this circumstance.

In the realm of dynamic systems, aggregate data refers to a data format in which the trajectory of each individual modeled by the evolution of state is not available, but rather a sample from the state distribution at a particular time point is available [16]. For example, the data collected for single-cell DNA sequence analysis, bird migration, and social gathering are aggregate data, as the individual trajectories for a long time are impossible to follow with only the collection of the states of different individuals obtained. In contrast, trajectory data includes all the individual information along the time. Thus, in other literature, trajectory and aggregate data are also called “paired” and “unpaired” data, respectively [17].

For trajectory data, there exist many methods developed such as Hamiltonian neural networks [18], Hidden Markov Model (HMM) [19], Kalman Filter (KF) [20], Particle Filter (PF) [21] and related works [16, 22]. Revealing determined hidden dynamics from data above can also be regarded as one special case of trajectory data when stochastic term vanishes. Thus, plenty of works investigate the trajectory data by revealing buried determined or under-determined dynamics from real data.

However, few works are investigated for aggregate data because of the absence of individual trajectories. By leveraging the Fokker-Planck equation, the governing function of the probability density function of the Winner process variable, researchers investigate the revealing hidden stochastic dynamics from aggregate data. Zhou *et al.* propose a novel method using the weak form of the Fokker Planck Equation (FPE), a partial differential equation, to describe the density evolution of data in a sampled form, which is then combined with the Wasserstein generative adversarial network (WGAN) in the training process [23]. Chen *et al.* proposed a method that leverages the physical-informed structure of Fokker-Planck equations and the approximation of the probability density function and reveals the hidden dynamics from samples in several time snapshots [24]. Liu *et al.* [17] integrated the distance measure such as Wasserstein distance used in WGAN [25] and the forward numerical solution of the parameterized stochastic differential equations as the Physics-Informed Deep Generative Models to reveal the hidden dynamics of the data.

In this work, leveraging the weak form of the Fokker-Planck equation, we proposed a Weak Collocation Regression (WCR) method to reveal the hidden stochastic dynamics from nonequally-spaced temporal aggregate data. The Fokker-Planck equation describes the time evolution of the

probability density function of the random variable in the Brownian motion. By the weak form of the Fokker-Planck equation, one can reduce the aggregate data to the low dimensional temporal sequence where the drift and diffusion term information is buried. A Monte-Carlo sum is introduced to calculate the weak form with a gaussian kernel as the test function. Temporal derivatives are reduced by Linear Multistep Methods (LMMs), and then the linear system constructed by collocation of the kernels gives an exact approximation of the stochastic dynamics. The benefits are three folds.

1. Comparable performance. Our method has a low computational cost, comparable accuracy, and restrained error, and the dimensional curse can be lessened. Numerical experiments show that the 1-dimensional problem can be easily revealed within 0.02 second on MacBook, while the computational time of the three or 4-dimensional problem can be limited to seconds. We can significantly reduce the error by changing the time interval and sample number. Directly numerically solving the inverse problem of stochastic differential equations may encounter the curse of dimensionality [26], where the tendency of numerical techniques requires a high computational cost growing exponentially with respect to the dimension of the variables. Benefits from the Monte-Carlo summation and the random collocations methods, the curse of dimensionality is lessened. Further, our method has natural potential for parallel computation, which also reduces the cost.
2. Robustness in different quality Data. Our method can handle a small amount of non-equally noise data without trajectory information and even partially missing. No trajectories are needed; the only thing needed is the summation of all the points at each given time. Our method hence has natural permutation invariance with respect to the observations of different individuals at the same time snapshot. The measurement error can be reduced to a great extent since the summation of the aggregate data is resistant to white noise. Partially missing data is allowed because we only require the summation over each time snapshot. Numerical experiments illustrate the stability of our methods against random noise. Without trajectories, the method can also be applied to different numbers of individuals at different time snapshots.
3. Complex tasks. Our method can overcome the coupled drift term derived from Sombbrero potential, variable-dependent diffusion term, and high-contrast problem and can be extended to a broader range. Numerical experiments show that it obtained the same result if we expanded each drift and diffusion term in a high-order polynomial. It shows that in dealing with the complex task above, our method has a broader representation and shows superior performance in revealing the hidden dynamics with a mild amount of data and high accuracy.

## 2 Methodology

In this paper, we consider the scenarios of the so-called aggregate data or unpaired data in some literature, where the trajectory information of each individual modeled by the evolution of the state is unavailable. Only the collection of the  $N_{t_j}$  samples  $\mathbb{X}_{t_j} = \{\mathbf{x}_{t_j}^i\}_{i=1}^{N_{t_j}}$  from the distribution of state  $X_t$  at certain time point  $t_j, j = 1, 2, \dots, L$  is available, i.e., the snapshots.

For simplicity, we denote the set of the aggregate data as

$$\mathbb{X} \triangleq \{\mathbb{X}_{t_j}\}_{j=1}^L = \{\{\mathbf{x}_{t_j}^i\}_{i=1}^{N_{t_j}}\}_{j=1}^L, \quad (1)$$

where  $t_j$  is the time index of the  $j$ -th snapshot in the total  $L$  snapshots,  $\mathbf{x}_{t_j}^i$  is the  $i$ -th sample of the variable  $X_t$  at time  $t_j$ . To model the stochastic dynamics of the data, the general stochastic

differential equations (SDEs) for Brownian motion are considered

$$dX_t = \boldsymbol{\mu}(X_t, t)dt + \boldsymbol{\sigma}(X_t, t)dW_t, \quad (2)$$

with drift term  $\boldsymbol{\mu}(X_t, t) \in \mathbb{R}^d$  and diffusion term  $\boldsymbol{\sigma}(X_t, t) \in \mathbb{R}^{d \times w}$ . Here,  $X_t$  is the  $d$ -dimensional random variable of the data, and  $W_t$  is the  $w$ -dimensional standard Brownian motion.

The density function  $p(x, t)$  of the above random variable  $X_t$  can be described by the Fokker-Planck equation (FP), see [27], and we restate the result in Lemma 1.

**Lemma 1.** *Suppose  $\{X_t\}$  solves the SDEs (2), then the possibility density function  $p(x, t)$  of the random variable  $X_t$  satisfies the following  $d$ -dimensional Fokker-Planck equation by the Itô integral*

$$\partial_t p = -\nabla \cdot (\boldsymbol{\mu}p) + \sum_{i,j} \partial_{ij}(D_{ij}p), \quad (3)$$

where  $\boldsymbol{x} \in \Omega \subset \mathbb{R}^d$ ,  $t \in [0, T] \subset \mathbb{R}$ ,  $p = p(\boldsymbol{x}, t) \in \mathbb{R}$  is the probability density function with  $\int_{\Omega} p(\boldsymbol{x}, t)dx = 1$ ,  $\boldsymbol{\mu} = [\mu_1(\boldsymbol{x}, t), \mu_2(\boldsymbol{x}, t), \dots, \mu_d(\boldsymbol{x}, t)]^T$ , and the diffusion matrix  $[D_{ij}] = [D_{ij}(\boldsymbol{x}, t)]$  is given by

$$D = \frac{1}{2} \boldsymbol{\sigma} \boldsymbol{\sigma}^T. \quad (4)$$

The Fokker-Planck equation bridges the gap between stochastic dynamics and the distributions of the data samples by sharing drift term and diffusion relation in SDE (2) and FP equation (3). To reveal the hidden stochastic dynamics (2), one can reveal the unknown terms in FP equation (3) by the samples following the corresponding probability distribution.

However, there is a huge gap between the density function and the data samples. Directly modeling the data by the Fokker-Planck equation usually needs the temporal and spatial derivatives of the density function  $p(t, x)$  with respect to  $t$  and  $x$ , requiring a large number of samples for constructing the smooth density function. It becomes even impossible to construct the smooth density function when the dimension increases. To overcome this difficulty, in this work, we propose a framework using the weak form with collocation integral kernels instead of reconstructing density function to fast reveal hidden stochastic dynamics with a mild amount of data. We briefly introduce the methods here. With the weak form, the partial derivatives moved to the explicit kernel function by integration by parts, making the computation of the spatial derivatives much easier. Followed by the Monte-Carlo summation, the integration over space can be given by the summation over the samples. Moreover, the terms with temporal derivatives can be well reduced by the linear multistep method (LMMs). Finally, the linear system is built with a basis expansion of the unknown drift and diffusion, and the sparse regression approximates the unknown terms. Figure 1 exhibits the picture of the methodology.

The weak form, LMMs, and the regression model will be discussed in detail in the following several subsections.

## 2.1 Leverage the weak form of the Fokker-Planck equation

In PDE theories, weak solutions from the weak form of PDEs are vital in analysis; see Evans' book [28] for detail. The weak form is introduced to solving PDEs with neural networks by the so-called WAN method [29] and then extended to reveal the unknown parameters in PDEs [30]. Borrowing the ideas from the Galerkin methods, we alter the FP equations' weak form by using the kernel function collocations as test functions. The generalities of test functions are approximately fulfilled through the kernel collocation, unlike the max update of the test function in WAN. Without maximum

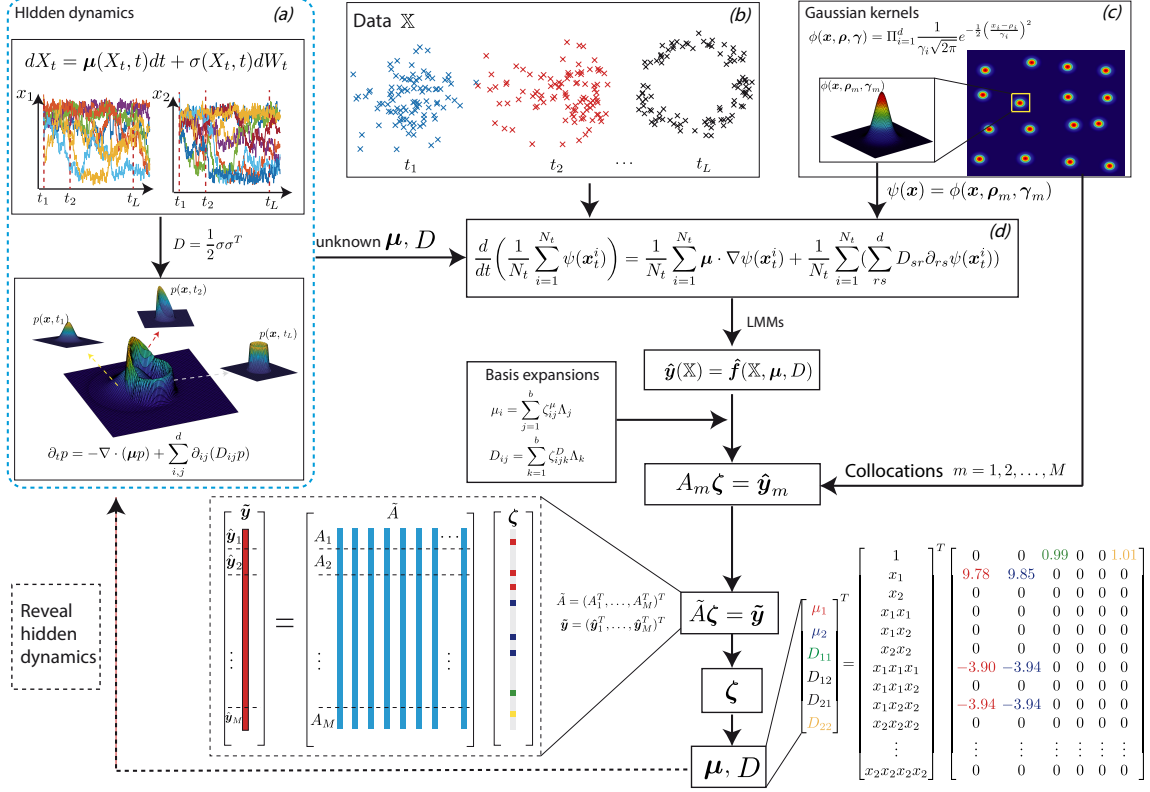


Figure 1: The diagram of the weak collocation regression method. The aggregate data set  $\mathbb{X}$  on panel (b) is the collection of  $L$  snapshots of samples at time  $t_1, t_2, \dots, t_L$  from one unknown stochastic process. We model this process by the stochastic differential equations in panel (a) with unknown drift  $\boldsymbol{\mu}(X_t, t)$  and diffusion  $\sigma(X_t, t)$  terms. By sampling Gaussian kernels in panel (c), the weak form in panel (d) gives the algebraic relation of the unknown terms and the data set for each kernel. By the LMMs and the expansion of the unknown terms, a linear system is built and further combined together to form a large system over all of the collocation kernels. Finally, the STRidge method gives the sparse regression of the drift and diffusion terms; hence, the hidden dynamics are revealed.

optimization for the test function, minimum optimization for the unknown terms in the dynamics achieves a more stable performance with high robustness.

The kernel function  $\psi(x) : \mathbb{R}^d \rightarrow \mathbb{R}$  is given as the test function. For example, a typical choice can be the Gaussian function with the form

$$\phi(\mathbf{x}, \boldsymbol{\rho}, \boldsymbol{\gamma}) = \prod_{i=1}^d \frac{1}{\gamma_i \sqrt{2\pi}} e^{-\frac{1}{2} \left( \frac{x_i - \rho_i}{\gamma_i} \right)^2}, \quad (5)$$

where  $\mathbf{x} = (x_1, \dots, x_d)^T \in \Omega$ ,  $\boldsymbol{\rho} = (\rho_1, \dots, \rho_d)^T$  and  $\boldsymbol{\gamma} = (\gamma_1, \dots, \gamma_d)^T$  are the expectation and standard deviation of the Gaussian function.

Multiply  $\psi(\mathbf{x})$  on both sides of equation (3), integrate by parts, and one obtains

$$\frac{d}{dt} \int_{\Omega} p(\mathbf{x}, t) \psi(\mathbf{x}) d\mathbf{x} = \int_{\Omega} p(\mathbf{x}, t) \boldsymbol{\mu}(\mathbf{x}, t) \cdot \nabla \psi(\mathbf{x}) d\mathbf{x} + \int_{\Omega} p(\mathbf{x}, t) \sum_{rs} D_{sr} \partial_{rs} \psi(\mathbf{x}) d\mathbf{x}, \quad (6)$$

where  $\partial_{rs} = \frac{\partial^2}{\partial x_r \partial x_s}$  and  $r, s$  are indices of the dimension. Here we have used the fact that  $p(x, t)|_{\partial\Omega} \rightarrow 0$  holds for the large enough domain  $\Omega$ .

As  $p(\mathbf{x}, t)$  is the density of the variable  $X_t$  at time  $t$  with  $\int p(\mathbf{x}, t) d\mathbf{x} = 1$ , we can rewrite equation (6) as the expectation form

$$\frac{d}{dt} \mathbb{E}_{\mathbf{x} \sim p(\mathbf{x}, t)}[\psi(\mathbf{x})] = \mathbb{E}_{\mathbf{x} \sim p(\mathbf{x}, t)}[\boldsymbol{\mu}(\mathbf{x}, t) \cdot \nabla \psi(\mathbf{x})] + \mathbb{E}_{\mathbf{x} \sim p(\mathbf{x}, t)}\left[\sum_{rs} D_{sr} \partial_{rs} \psi(\mathbf{x})\right], \quad (7)$$

where  $\mathbb{E}_{\mathbf{x} \sim p(\mathbf{x}, t)}$  is the expectation over the probability density function  $p(\mathbf{x}, t)$ .

## 2.2 Approximate the weak form using data

In the scenarios of real applications, the probability distribution  $p(\mathbf{x}, t)$  is hard to obtain, but the data of many samplings from the distribution is always feasible, thanks to modern technology and instruments. By the law of large numbers, the expectation over the distribution can be approximated by the summation over the samplings of the variable related to the distribution, i.e.,

$$\frac{1}{N_t} \sum_{i=1}^{N_t} \psi(\mathbf{x}_t^i) \sim \mathbb{E}_{\mathbf{x} \sim p(\mathbf{x}, t)}[\psi(\mathbf{x})], \quad (8)$$

where  $N_t$  is the number of the samplings of the variable  $X_t$  at time  $t$ , and  $\mathbf{x}_t^i$  is the  $i$ -th sampling.

For simplicity, we denote the data set over time as  $\mathbb{X}_t \triangleq \{\mathbf{x}_t^i\}_{i=1}^{N_t}$ . Thus, with the data set of the samplings  $\mathbb{X}_t$ , the weak form of the FP equation (3) yields

$$\frac{d}{dt} \left( \frac{1}{N_t} \sum_{i=1}^{N_t} \psi(\mathbf{x}_t^i) \right) = \frac{1}{N_t} \sum_{i=1}^{N_t} \boldsymbol{\mu}(\mathbf{x}_t^i, t) \cdot \nabla \psi(\mathbf{x}_t^i) + \frac{1}{N_t} \sum_{i=1}^{N_t} \left( \sum_{rs} D_{sr} \partial_{rs} \psi(\mathbf{x}_t^i) \right) + \epsilon, \quad (9)$$

where we have used the approximations of the expectations by the summations of the samples and the discussion of the error term  $\epsilon$  can be found in the appendix. The drift and diffusion information is related to the data set  $\mathbb{X}_t$  in equation (9). The dimension of the data has been reduced to one by the summation over the samplings with only the dependence on the time  $t$  left. This form reveals that our method is naturally suited for the high-dimensional problem.

For simplicity, we denote

$$\frac{d}{dt}y(\mathbb{X}_t) = f(\mathbb{X}_t, \boldsymbol{\mu}, D), \quad (10)$$

where

$$y(\mathbb{X}_t) = \frac{1}{N_t} \sum_{i=1}^{N_t} \psi(\mathbf{x}_t^i)$$

and

$$f(\mathbb{X}_t, \boldsymbol{\mu}, D) = \frac{1}{N_t} \sum_{i=1}^{N_t} \boldsymbol{\mu}(\mathbf{x}_t^i, t) \cdot \nabla \psi(\mathbf{x}_t^i) + \frac{1}{N_t} \sum_{i=1}^{N_t} \left( \sum_{rs}^d D_{sr} \partial_{rs} \psi(\mathbf{x}_t^i) \right)$$

are scalar functions varying over time  $t$ .

### 2.3 Approximate the temporal derivatives

We show a method like Tikhonov differentiation to directly calculate the derivatives in the appendix because its results have a certain gap with the method used in the text. Other than considering the approximation of the derivatives, we note that the equation (10) is a 1-dimensional parameterized ordinary differential equation where the solutions on the discrete times were given with  $y(\mathbb{X})$ . The inverse problem of finding unknown terms in the FP equation now reduces to the inverse problem of the 1-dimensional ordinary differential equation (10). Many methods recently have been developed to reveal the dynamics such as SINDy [31], PINN [6] and ODENet [8]. Considering the simplicity, in this work, we use the implicit form of Linear Multistep Methods (LMMs) here to construct an explicit form of equation (10).

Linear Multistep Methods (LMMs) have been developed as popular numerical schemes for the integration of the ordinary differential equations for the known dynamic systems [32] with well-established mathematical theories [33]. Raissi *et al.* constructed multistep neural networks for the data-driven discovery of nonlinear dynamical systems leveraging LMMs [34]. Recently Du *et al.* applied LMMs in learning hidden dynamics from the data of a given state with theoretical analysis of the stabilities and the convergence for the inverse problem [35, 23]. In their work, an equally-spaced version of LMMs is used. However, real data in the record usually contain many missing points and flaws, making the equally-spaced version of LMM hard to apply. In this work, with the help of variable step size Adams methods [36], we can deal with the non-equally spaced temporal data for the discovery of the hidden dynamics.

For equally-spaced temporal data, Implicit Adams methods of trapezoidal rule, Milne method, 2-step backward differentiation method (BDF2), and Adams-Moulton methods are used in this work, some of them are listed below, and others can be found in the appendix.

$$\text{Trapezoidal rule: } y_{n+1} - y_n = \frac{h}{2}(f_{n+1} + f_n), \quad (11)$$

$$\text{Milne method: } y_{n+1} - y_{n-1} = \frac{h}{3}(f_{n+1} + 4f_n + f_{n-1}), \quad (12)$$

where  $y_n = y(t_n)$ ,  $f_n = f(t_n, \theta)$  and  $h \equiv h_n = t_{n+1} - t_n$  for  $n = 1, 2, \dots, L - 1$ .

For more general temporal data without equally spaced time, the 2-step BDF-formula of variable step size methods is as follows

$$y_{n+1} - \frac{(1 + \omega_n)^2}{1 + 2\omega_n} y_n + \frac{\omega_n^2}{1 + 2\omega_n} y_{n-1} = h_n \frac{1 + \omega_n}{1 + 2\omega_n} f_{n+1}, \quad (13)$$

where  $\omega_n = h_n/h_{n-1}$ .

Recall that the Implicit Adams methods of the trapezoidal rule require only two adjacent time points. Thus the variable step-size version reads

$$y_{n+1} - y_n = \frac{h_n}{2}(f_{n+1} + f_n). \quad (14)$$

Our numerical experiments show that the one-step rule of the LMMs performs well when the samples on only three-time snapshots are available. In contrast, the LMMs methods requiring two steps fail in such a scenario even if they have a higher order of accuracy. Other numerical schemes, e.g., the schemes listed in the appendix, have also been tested but with a worse performance than the LMMs.

Either by Tikhonov differentiation or the LMMs, we derive the discrete form of equation (10) as the following form

$$\hat{\mathbf{y}}(\mathbb{X}) = \hat{\mathbf{f}}(\mathbb{X}, \boldsymbol{\mu}, D), \quad (15)$$

where  $\hat{\mathbf{y}}(\mathbb{X})$  is a vector constructed by  $\mathbf{y}(\mathbb{X}) = \{y(\mathbb{X}_{t_j})\}_{j=1}^L$ , and  $\hat{\mathbf{f}}(\mathbb{X}, \boldsymbol{\mu}, D)$  is a vector with the same size given by  $\mathbf{f}(\mathbb{X}, \boldsymbol{\mu}, D) = \{f(\mathbb{X}_{t_j}, \boldsymbol{\mu}, D)\}_{j=1}^L$ . Now the equation (15) gives us an algebraic equation, from which, by an apt ansatz form for the drift and diffusion terms, we can reveal  $\boldsymbol{\mu}$  and  $D$  with the data set  $\mathbb{X}$ . Although we list Tikhonov differentiation in the appendix, it is much worse than LMMs in our experiments. Thus, we omit the results leveraging the Tikhonov differentiation.

## 2.4 Build the regression model

In this subsection, we investigate the sparse regression and collocations of the kernels to solve  $\boldsymbol{\mu}$  and  $D$  from (15) with the data set  $\mathbb{X}$ . The polynomial expressions are adopted for approximating the drift and diffusion terms, with the basis coefficients to be determined. Let

$$\Lambda = \{1, x_1, x_2, \dots, x_d, x_1x_1, x_1x_2, \dots, x_d^p\}^T \quad (16)$$

denote the  $p$ -th order complete polynomials with respect to the variable  $\mathbf{x} = (x_1, \dots, x_d)^T$ . The number of the terms of  $\Lambda$  is  $b \triangleq |\Lambda| = \binom{p+d}{p}$ . Here, for simplicity, we suppose that  $\boldsymbol{\mu}$  and  $D$  are independent of  $t$ . And the components  $\mu_i$  of  $\boldsymbol{\mu} = [\mu_i]$  and  $D_{ij}$  of  $D = [D_{ij}]$  expand as

$$\mu_i = \sum_{j=1}^b \zeta_{ij}^\mu \Lambda_j, \quad \text{and} \quad D_{ij} = \sum_{k=1}^b \zeta_{ijk}^D \Lambda_k, \quad (17)$$

where  $\Lambda_j$  is the  $j$ -th component in the basis set  $\Lambda$ .

Now, equation (10) has the following matrix form

$$\frac{d}{dt} \mathbf{y}(\mathbb{X}) = B(\mathbb{X}) \boldsymbol{\zeta} \quad (18)$$

where

$$\boldsymbol{\zeta} = \underbrace{\{\zeta_{11}^\mu, \dots, \zeta_{1b}^\mu, \dots, \zeta_{d1}^\mu, \dots, \zeta_{db}^\mu\}}_{\text{flatten of } \boldsymbol{\zeta}^\mu} \underbrace{\{\zeta_{111}^D, \dots, \zeta_{11b}^D, \dots, \zeta_{dd1}^D, \dots, \zeta_{ddb}^D\}}_{\text{flatten of } \boldsymbol{\zeta}^D}^T, \quad (19)$$

and the flatten scheme of  $\zeta^\mu$  and  $\zeta^D$  is shown as

$$\zeta^\mu : \begin{pmatrix} \zeta_{11}^\mu & \zeta_{12}^\mu & \cdots & \zeta_{1b}^\mu \\ \zeta_{21}^\mu & \zeta_{22}^\mu & \cdots & \zeta_{2b}^\mu \\ \cdots & \cdots & \cdots & \cdots \\ \zeta_{d1}^\mu & \zeta_{d2}^\mu & \cdots & \zeta_{db}^\mu \end{pmatrix}, \quad \zeta^D : \begin{pmatrix} \zeta_{11b}^D & \zeta_{d1b}^D \\ \zeta_{112}^D & \zeta_{d12}^D \\ \zeta_{111}^D & \zeta_{d11}^D \\ \zeta_{1db}^D & \zeta_{ddb}^D \\ \zeta_{1d2}^D & \zeta_{dd2}^D \\ \zeta_{1d1}^D & \zeta_{dd1}^D \end{pmatrix}$$

and  $B(\mathbb{X}) := \begin{pmatrix} \mathbf{b}_1^T(\mathbb{X}) \\ \vdots \\ \mathbf{b}_L^T(\mathbb{X}) \end{pmatrix}$  is a known coefficient matrix with size  $L \times (db + d^2b)$ ,  $\mathbf{y}(\mathbb{X}) := \begin{pmatrix} y_1(\mathbb{X}) \\ \vdots \\ y_L(\mathbb{X}) \end{pmatrix}$  is a column vector with size  $L$ .

By applying linear multistep methods (LMMs) on the temporal derivative in (18), one can obtain a linear system about the coefficient vector  $\zeta$  as

$$A(\mathbb{X})\zeta = \hat{\mathbf{y}}(\mathbb{X}), \quad (20)$$

where  $A(\mathbb{X})$  and  $\hat{\mathbf{y}}(\mathbb{X})$  are constructed by  $B(\mathbb{X})$  and  $\mathbf{y}(\mathbb{X})$  in (18) because of the linearity of the system, and the coefficient vector  $\zeta$  are collected and vectorized from all the coefficients  $\left\{ \left\{ \zeta_{ij}^\mu \right\}_{j=1}^b \right\}_{i=1}^d$  and  $\left\{ \left\{ \zeta_{ijk}^D \right\}_{k=1}^b \right\}_{i,j=1}^d$  in the expansions of  $\mu$  and  $D$  shown in (19). Now, equation (20) gives the relation between the data set  $\mathbb{X}$  and the unknown parameters in the polynomial expansions of the hidden dynamics.

**Example 1.** To clarify, we give an example of how the linear system is obtained by applying LMMs such as the trapezoidal rule (11) on the equation (18) with temporal derivatives. By the trapezoidal rule, the  $i$ -th row vector  $\mathbf{a}_i^T(\mathbb{X})$  of the matrix  $A(\mathbb{X})$  and the  $i$ -th scalar  $\hat{y}_i(\mathbb{X})$  of the vector  $\hat{\mathbf{y}}(\mathbb{X})$  are calculated as follows

$$\mathbf{a}_i^T(\mathbb{X}) = \frac{h}{2}(\mathbf{b}_i^T(\mathbb{X}) + \mathbf{b}_{i+1}^T(\mathbb{X})), \quad \hat{y}_i(\mathbb{X}) = y_{i+1}(\mathbb{X}) - y_i(\mathbb{X}), \quad i = 1, 2, \dots, L-1 \quad (21)$$

Hence, the matrix  $A(\mathbb{X}) \in \mathbb{R}^{(L-1) \times (db+d^2b)}$  and vector  $\hat{\mathbf{y}}(\mathbb{X}) \in \mathbb{R}^{L-1}$  in the linear system can be assembled by

$$A(\mathbb{X}) := \begin{pmatrix} \mathbf{a}_1^T(\mathbb{X}) \\ \vdots \\ \mathbf{a}_{L-1}^T(\mathbb{X}) \end{pmatrix} \quad \text{and} \quad \hat{\mathbf{y}}(\mathbb{X}) := \begin{pmatrix} \hat{y}_1(\mathbb{X}) \\ \vdots \\ \hat{y}_{L-1}(\mathbb{X}) \end{pmatrix}. \quad (22)$$

Here, the rows of the matrix  $A(\mathbb{X})$  or the elements of the vector  $\hat{\mathbf{y}}(\mathbb{X})$  are constructed by the rows of  $B(\mathbb{X})$  or the elements of  $\mathbf{y}(\mathbb{X})$  where the number of rows is reduced by one because of the trapezoidal rule.

A sparse regression applied to the linear system then reveals the data's hidden dynamics. However, before that, we would discuss the collocation strategies to improve the robustness and accuracy. Recall that in this work, the test function  $\psi$  is considered as the Gaussian function  $\psi = \phi(\mathbf{x}, \boldsymbol{\rho}, \boldsymbol{\gamma}) \triangleq \prod_{i=1}^d \frac{1}{\gamma_i \sqrt{2\pi}} e^{-\frac{1}{2} \left( \frac{x_i - \rho_i}{\gamma_i} \right)^2}$  given by (5), one can easily obtain the the specific form of the linear system (20) as

$$A(\mathbb{X}, \boldsymbol{\rho}, \boldsymbol{\gamma})\boldsymbol{\zeta} = \hat{\boldsymbol{y}}(\mathbb{X}, \boldsymbol{\rho}, \boldsymbol{\gamma}) \quad (23)$$

by the replacement of  $\psi(x) = \phi(\mathbf{x}, \boldsymbol{\rho}, \boldsymbol{\gamma})$ .

The collections of the test functions is taken as  $\mathbb{C}_{\boldsymbol{\rho}, \boldsymbol{\gamma}}^d = \{\phi(\cdot, \boldsymbol{\rho}_m, \boldsymbol{\gamma}_m)\}_{m=1}^M$  where  $\boldsymbol{\rho}_m \in \mathbb{R}^d$  and  $\boldsymbol{\gamma}_m \in \mathbb{R}^d$ . Taking the  $m$ -th Gaussian function  $\phi(\cdot, \boldsymbol{\rho}_m, \boldsymbol{\gamma}_m)$  as the test function, the linear system with respect to  $\boldsymbol{\zeta}$  yields

$$A_m \boldsymbol{\zeta} = \hat{\boldsymbol{y}}_m, \quad (24)$$

where  $A_m = A(\mathbb{X}, \boldsymbol{\rho}_m, \boldsymbol{\gamma}_m)$  and  $\hat{\boldsymbol{y}}_m = \hat{\boldsymbol{y}}(\mathbb{X}, \boldsymbol{\rho}_m, \boldsymbol{\gamma}_m)$ . The values of the unknown coefficients  $\boldsymbol{\zeta}$  can be revealed by solving this linear system. However, integral with one test function  $\phi(\mathbf{x}, \boldsymbol{\rho}_i, \boldsymbol{\gamma}_i)$  reveals only part of the information from the given data. Hence, we build the linear systems over the whole test function collection  $\mathbb{C}_{\boldsymbol{\rho}, \boldsymbol{\gamma}}^d$ . Namely, we solve the linear equation

$$\tilde{A} \boldsymbol{\zeta} = \tilde{\boldsymbol{y}}, \quad (25)$$

where

$$\tilde{A} = \begin{pmatrix} A_1 \\ A_2 \\ \vdots \\ A_M \end{pmatrix}, \text{ and } \tilde{\boldsymbol{y}} = \begin{pmatrix} \hat{\boldsymbol{y}}_1 \\ \hat{\boldsymbol{y}}_2 \\ \vdots \\ \hat{\boldsymbol{y}}_M \end{pmatrix} \quad (26)$$

are constructed by the matrix  $\{A_m\}_{m=1}^M$  and the vector  $\{\hat{\boldsymbol{y}}_m\}_{m=1}^M$  over all of the test functions in the collection  $\mathbb{C}_{\boldsymbol{\rho}, \boldsymbol{\gamma}}^d$ .

To better approximate the entire test functional space, the collection  $\mathbb{C}_{\boldsymbol{\rho}, \boldsymbol{\gamma}}^d$  needs to be large enough, which means a huge amount of computational cost. To overcome this difficulty, we borrow the ideas of the functional basis from the Galerkin methods and the collocation points from the collocation methods. It is key to generate the collection of the test functions  $\mathbb{C}_{\boldsymbol{\rho}, \boldsymbol{\gamma}}^d$  taking into account the efficiency and the accuracy. For simplicity, we randomly generate  $M$  parameters of  $\boldsymbol{\rho}_m$  in the range of the values of the data  $\mathbb{X}$ . And the uniform standard derivation parameter  $\boldsymbol{\gamma}_m = \mathbf{1}$  is taken. Thus the test function collection  $\mathbb{C}_{\boldsymbol{\rho}, \boldsymbol{\gamma}}^d$  is obtained and the large linear system (25) is then built.

Followed by the linear regression and sparse identification algorithm (STRidge) [7], the explicit form of the solved dynamics fits the data. Specifically, to give the sparse results, the linear regression is applied but with the hard threshold  $\eta$  taken, i.e., the minor component of  $\boldsymbol{\zeta}$  less than  $\eta$  would be set zero, and then the linear regression continues until converges. Distributing the components of  $\boldsymbol{\zeta}$  to the drift and diffusion terms gives the explicit form of the hidden stochastic dynamics.

The pseudo-code of the algorithm is exhibited in Algorithm 1. Figure 1 shows the whole procedure of the methodology.

**Remark 1.** *Another choice of the ansatz for the drift and diffusion terms can be the neural network because of its so-called universal approximation properties. However, it would require nonlinear optimization, which enhances the complexity of the algorithm, and left for further investigations beyond the scope of this work. We focus on introducing the framework of the weak form to reveal the hidden dynamics in this work.*

---

**Algorithm 1:** Weak Collocation Regression method (WCR).

---

**Result:** The explicit form of the governing stochastic equation of the data.

**Input:** Aggregate data set  $\mathbb{X}$ .

- 1 Sample  $M$  expectations  $\{\boldsymbol{\rho}_m\}_{m=1}^M$  in the region  $\Omega$  which contains all of the samples in the data set  $\mathbb{X}$ ;
- 2 Set the expectations  $\{\boldsymbol{\gamma}_m\}_{m=1}^M$  as hyper-parameters with default 1 in each dimension;
- 3 Generate the Gaussian function collections  $\mathbb{C}_{\boldsymbol{\rho}, \boldsymbol{\gamma}}^d = \{\phi(\cdot, \boldsymbol{\rho}_m, \boldsymbol{\gamma}_m)\}_{m=1}^M$  using above expectations and derivations;
- 4 **for**  $m \leq M$  **do**

- 5 Compute and assemble the vector  $\mathbf{y}(\mathbb{X}) = \begin{pmatrix} \vdots \\ \frac{1}{N_{t_l}} \sum_{i=1}^{N_{t_l}} \phi(\mathbf{x}_{t_l}^i, \boldsymbol{\rho}_m, \boldsymbol{\gamma}_m) \\ \vdots \end{pmatrix}$  by the left term

of the weak form (9) where the test function  $\psi = \phi(\mathbf{x}_{t_l}^i, \boldsymbol{\rho}_m, \boldsymbol{\gamma}_m)$  and  $l$  is the index of the  $l$ -th time snapshots;

- 6 Compute and assemble the matrix  $B(\mathbb{X})$  in (18) by the right term of the weak form (9) over all of the time snapshots with the help of the polynomial basis expansions of each entry of drift vector  $\boldsymbol{\mu} = [\mu_i]$  and diffusion matrix  $D = [D_{ij}]$

$$\mu_i = \sum_{j=1}^b \zeta_{ij}^\mu \Lambda_j, \quad \text{and} \quad D_{ij} = \sum_{k=1}^b \zeta_{ijk}^D \Lambda_k;$$

- 7 Assemble the vector  $\boldsymbol{\zeta}$  by  $\boldsymbol{\zeta}^\mu = [\zeta_{ij}^\mu]$  and  $\boldsymbol{\zeta}^D = [\zeta_{ijk}^D]$  using the flatten scheme in (19);
- 8 Compute the matrix  $A_m$  and  $\hat{\mathbf{y}}_m$  by the matrix  $B(\mathbb{X})$  and  $\mathbf{y}(\mathbb{X})$  using the LMMs, e.g., the trapezoidal rule (11);
- 9 **end**

- 10 Construct the large linear system  $\tilde{A}\boldsymbol{\zeta} = \tilde{\mathbf{y}}$  with  $\tilde{A} = (A_1^T, \dots, A_M^T)^T$  and  $\tilde{\mathbf{y}} = (\hat{\mathbf{y}}_1^T, \dots, \hat{\mathbf{y}}_M^T)^T$ ;
  - 11 Compute  $\boldsymbol{\zeta}$  by a sparse linear regression of  $\tilde{A}\boldsymbol{\zeta} = \tilde{\mathbf{y}}$ ;
  - 12 Reconstruct the drift  $\boldsymbol{\mu}$  and diffusion  $D$  with the solved coefficient  $\boldsymbol{\zeta}$ .
- 

### 3 Numerical experiments

**Data acquisition.** All the raw data used in this work for the experiments of revealing the hidden dynamics are obtained by integrating the given SDEs

$$dX_t = \boldsymbol{\mu}_t dt + \boldsymbol{\sigma}_t dW_t, \quad t \geq 0$$

from  $t = 0$  to  $t = T$  with Euler-Maruyama scheme

$$\tilde{X}_{(i+1)\delta t} = \tilde{X}_{i\delta t} + \boldsymbol{\mu}_t \delta t + \boldsymbol{\sigma}_t \sqrt{\delta t} \mathcal{N}_i. \quad (27)$$

Here  $\delta t$  is the time step of the numerical scheme,  $\mathcal{N}_i$  are i.i.d standard Gaussian random variables, and the initial values are sampled from a given distribution such as a Gaussian function. The same random seed is adopted among different experiments. The experimental data is then sampled from these trajectories, i.e.,  $N_i$  points are sampled at each time snapshot to remove the trajectory information, and only  $L$  time snapshots are chosen as the experimental data, denoted as  $\mathbb{X} =$

$\{\mathbb{X}_i\}_{i=1}^L = \{\{\mathbf{x}_i^j\}_{j=1}^{N_i}\}_{i=1}^L$ . The time snapshots can be non-equally spaced where the time interval  $\Delta t_i = t_{i+1} - t_i$  varies, and if the time interval is equal, we denote the interval as  $\Delta t$ . The random noise is added to the raw data with the noise level  $\delta$  as  $\hat{\mathbf{x}}_i^j = \mathbf{x}_i^j + \delta \mathcal{U}_i^j \mathbf{x}_i^j$  where  $\mathcal{U}_i^j$  is a random variable.

**Experimental setups.** In this work, we use the collocations of the Gaussian functions as the test functions for the weak form. We sample these Gaussian kernels by randomly sampling the expectations  $\boldsymbol{\rho}_m$ ,  $m = 1, 2, \dots, M$  using Latin Hypercube Sampling method [37] in the region of the data, i.e., the hypercube containing all of the data. Moreover, the standard derivation  $\boldsymbol{\gamma} = \gamma I_d$ , where  $I_d$  is the identity matrix, is chosen as a hyperparameter with default  $\gamma = 1$  in each sampled Gaussian function. In all cases, our experiments show that all of the nonzero coefficients are correctly identified, and all of the zero terms are eliminated by the sparse regression. Hence in this work, we define the Maximum Relative Error (MRE) of nonzero terms

$$\text{MRE} = \max_{\theta_i \neq 0} \frac{|\hat{\theta}_i - \theta_i|}{|\theta_i|}$$

as the criterion for the evaluation of the experimental results, where  $\theta_i$  represents the  $i$ -th parameter of the drift and diffusion terms and  $\hat{\theta}_i$  is the learned parameter from data. All the experiments were done on the MacBook Pro 2021 with an M1 chip. We summarize the notations used throughout the experiments in Table 1.

Variable	definition	Variable	definition
$L$	Number of time snapshots	$\Delta t$	Time interval of snapshots
$\gamma$	Gaussian variance	$\boldsymbol{\rho}_m$	Expectation of the $m$ -th Gaussian kernel
$M$	Gaussian sample number	$N_i$	Sample number at $i$ -th time snapshot
MRE	Maximum Relative Error	$\delta$	Noise level

Table 1: Notations used throughout the experiments

### 3.1 Typical 1-dimensional problem

One-dimensional stochastic problem widely exists in the scientific and engineering fields, such as population growth, asset price, and investments [38]. To better illustrate the abilities of our WCR method for dealing with complex tasks, in this section, we focus on revealing the hidden dynamics from 1d aggregate data avoiding the difficulties brought by the dimension of the data. We consider the following 1d model

$$dX_t = \mu(X_t)dt + \sigma(X_t)dW_t, \quad (28)$$

where drift  $\mu(X_t)$  and diffusion  $\sigma(X_t)$  terms reduce to scalar functions. Here we mainly focus on the three cases: (I) Cubic polynomial problem with only three snapshots; (II) Variable-dependent diffusion problem; (III) Quintic polynomial problem with high contrast. Furthermore, these cases give a direct illustration of the good performance of WCR on complex tasks.

**(I) Cubic polynomial problem with three snapshots.** In this case, the raw data of the experiment are generated by the 1d cubic polynomial form

$$dX_t = (X_t - X_t^3)dt + dW_t \quad (29)$$

in from  $t = 0$  to  $t = 1$  with initial values at  $t = 0$  sampled from a Gaussian distribution  $\mathcal{N}(0, 0.1)$  using Euler-Maruyama scheme (27). We obtained 10,000 samples at each snapshot, and only three

snapshots at (a)  $t = 0.1, 0.3, 0.5$  and (b)  $t = 0.2, 0.5, 1$  are adopted as the experimental data. In this case, we expand the drift term as the third-order basis expansion form

$$\mu(x) = \lambda_0 + \lambda_1 x + \lambda_2 x^2 + \lambda_3 x^3,$$

and the diffusion term is treated as a tunable parameter  $D(x) = \frac{1}{2}\sigma^2 = D_0$ . We have used the same experimental setup for the same problem of Chen’s work [24].

Only three snapshots are available in the data set (a) and (b). Further, the time intervals of the snapshots in (b) are not equal. Thus the approximation of the temporal derivatives requires a reliable scheme to overcome the difficulties. Here we use the variable step-size version of Implicit Adams methods of trapezoidal rule (14), which can be applied to a small number of time snapshots and non-equally spaced time series data. For the collocation kernels, 20 Gaussian kernels are sampled by sampling the expectations of the Gaussian function using the LHS method with the standard variance set as  $\gamma = 0.85$ .

The results are shown in Figure 2 and Table 2. We have compared the results with Chen’s results [24] as state of the art (SOTA) to show that for the same problem, the WCR method can achieve a comparable accuracy but with a much less computational cost. All of the nonzero terms are correctly identified, and all of the zero terms are eliminated by the sparse regression. The MRE of (a) and (b) are less than 4.6% and 0.42%, respectively. Most notably, the experiments of applying WCR on the data set (a) and (b) are all completed within 0.02s on a MacBook Pro 2021 with an M1 chip.

For a mild amount of the data, the WCR method still achieves remarkable performances. We sampled 1000 points for each snapshot in case (b) above without changing other setups to test our framework. In this case, the WCR method still achieves a good result with the MRE less than 4% within only 0.006s on the MacBook pro.

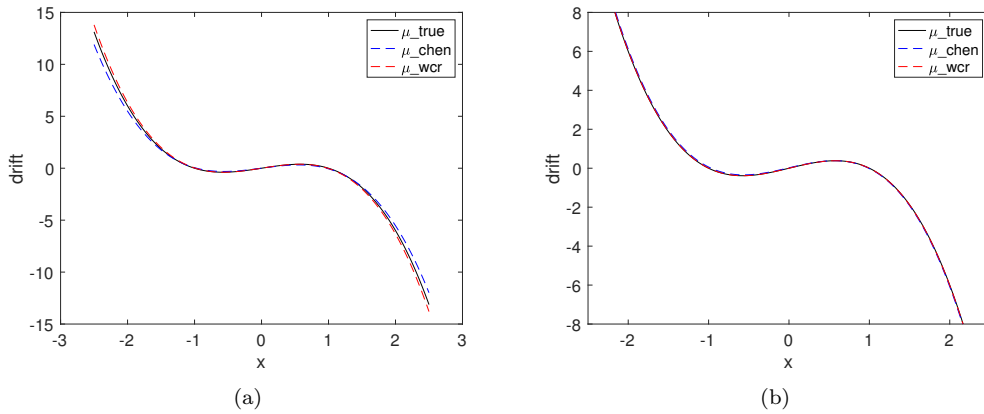


Figure 2: The results of 1d cubic polynomial problem compared with Chen’s work (SOTA). Reveal the unknown drift and diffusion terms with 10000 samples of  $X_t$  at different time snapshots: (a) Observations at  $t = 0.1, 0.3, 0.5$ ; (b) Observations at  $t = 0.2, 0.5, 1$  where the samples are generated by the given SDE with drift term  $\mu_{\text{true}} = x - x^3$  and diffusion term  $\sigma = 1$ . The inference results are denoted by  $\mu_{\text{chen}}$  (SOTA) and  $\mu_{\text{wcr}}$  (ours).

**(II) Variable-dependent diffusion term problem.** Much attention in the existing literature is paid to the problem of constant diffusion in revealing the hidden dynamics from data. However,

Parameter	$\lambda_0$	$\lambda_1$	$\lambda_2$	$\lambda_3$	$\sigma$
True parameters	0	1	0	-1	1
(a) Chen	0.0051	0.8422	-0.0071	-0.8994	1.0347
(a) WCR	0	<b>1.0160</b>	0	<b>-1.0457</b>	<b>1.0127</b>
(b) Chen	0.0225	0.9638	-0.0010	-1.0035	1.0138
(b) WCR	0	<b>0.9982</b>	0	<b>-1.0019</b>	<b>1.0042</b>

Table 2: The results of 1d cubic polynomial problem compared with Chen’s work (SOTA). Reveal the unknown drift and diffusion terms with 10000 samples of  $X_t$  at different time snapshots: (a) Observations at  $t = 0.1, 0.3, 0.5$ ; (b) Observations at  $t = 0.2, 0.5, 1$  where the samples are generated by the given SDE with drift term  $\mu_{\text{true}} = x - x^3$  and diffusion term  $\sigma = 1$ . The inference results are denoted by Chen (SOTA) and WCR (ours).

a more general setting is the non-constant diffusion, i.e., the variable-dependent diffusion. In this part, we will show that the WCR method also works for the variable-dependent case. The variable-dependent stochastic equation

$$dX_t = (X_t - X_t^3)dt + (1 + X_t)dW_t$$

is considered as the true model to generate the raw data of the snapshots at time  $t = 0, 0.2, 0.5, 1$ . Our task is to reveal the true model from the data by the parameterized SDE form

$$dX_t = (\lambda_0 + \lambda_1 X_t + \lambda_2 X_t^2 + \lambda_3 X_t^3)dt + (\sigma_0 + \sigma_1 X_t)dW_t, \quad (30)$$

where  $\lambda_i, i = 0, 1, 2, 3$  and  $\sigma_j, j = 0, 1$  are the tunable parameters. Note that the weak form of the Fokker-Planck is leveraged in our method, where the drift term  $\mu(x)$  and the  $1 \times 1$  diffusion matrix  $D$  are revealed. By setting  $D(x) = b_0 + b_1 x + b_2 x^2$ , WCR method gives the approximation of the values of  $\lambda_i, i = 0, 1, 2, 3$  and  $b_j, j = 0, 1, 2$ . And by the relation  $D = \frac{1}{2}\sigma^2$ , a nonlinear regression is applied on the diffusion matrix  $D$  and the parameters  $\sigma_i, i = 0, 1$  are approximated, giving the explicit form of the governing equation (30). The results of the parameters are listed in Table 3, and the WCR method still works well in the variable-dependent problem.

Parameter	$\lambda_0$	$\lambda_1$	$\lambda_2$	$\lambda_3$	$\sigma_0$	$\sigma_1$
True	0	1	0	-1	1	1
WCR	0	0.9688	0	-1.0264	0.9955	1.0326

Table 3: The results of 1d cubic polynomial problem when diffusion term is not a constant. Reveal the unknown drift and diffusion terms with 10000 samples of  $X_t$  at  $t = 0, 0.2, 0.5, 1$  where the samples are generated by the given SDE with drift term  $\mu_{\text{true}} = x - x^3$  and diffusion term  $\sigma = 1 + x$ .

**(III) Quintic polynomial drift problem.** Quintic polynomial drift has fifth-order polynomial terms, raising the difficulty of revealing the true form of the hidden stochastic dynamics. The problem becomes more subtle when the coefficients of the polynomial terms are on different scales. In this experiment, we would show that for the high order polynomial drift term with high contrast coefficient, the WCR method can still reach a good accuracy in modeling the data.

The raw data are generated by integrating the following SDE from  $t = 0$  to  $t = 10$

$$dX_t = \mu dt + dW_t, \quad (31)$$

where the drift term is the high order polynomial form with high contrast coefficient as

$$\mu \triangleq -x(x-1)(x-2)(x-3)(x-4) = -24x + 50x^2 - 35x^3 + 10x^4 - x^5. \quad (32)$$

In this experiment, WCR is applied to the aggregate data  $\mathbb{X}$  to reveal the hidden stochastic dynamics. Two kinds of the data with time interval (a)  $\Delta t = 0.1$  and (b)  $\Delta t = 0.5$  with  $N = 5000$  points in each time snapshot are considered. To model the data, we take the fifth order of the polynomial expansion for the drift term with

$$\mu(x) = \theta_0 + \theta_1 x + \theta_2 x^2 + \theta_3 x^3 + \theta_4 x^4 + \theta_5 x^5,$$

where  $\theta_i, i = 0, 1, \dots, 5$  are the tunable parameters to be determined by the data. The diffusion term is chosen as one tunable parameter  $D_0$ .

In the collocation of the kernels, 200 Gaussian functions are sampled by randomly generating their expectations  $\{\rho_i\}_{i=1}^{200}$  in the region of the data with the default standard variance  $\gamma = 1$ . For the approximation of the temporal derivatives, the Milne method is applied. The computation cost is within 2 seconds, and the results are summarized in Table 4. From the result, we can see that the WCR method achieves a good performance in the problem with less than 3% Max Relative Error (MRE) within seconds on the Macbook Pro.

Settings	drift coefficients $\{\theta_i\}_{i=0}^5$						diffusion $D_0$	MRE	Time (s)
True	0	-24	50	-35	10	-1	1	-	-
(a) $\Delta t = 0.1$	0	-23.8	49.6	-34.7	9.92	-0.991	1.002	0.87%	1.8
(b) $\Delta t = 0.5$	0	-24.9	51.6	-35.9	10.2	-1.018	1.029	3.82%	0.4

Table 4: The results of one-dimensional high contrast problem with different time snapshots. Reveal the unknown drift and diffusion terms with (a)  $\Delta t = 0.1$ ; (b)  $\Delta t = 0.5$ , where the samples are generated by the true SDE with drift term  $\mu(x) = -24x + 50x^2 - 35x^3 + 10x^4 - x^5$  and diffusion term  $\sigma = 1$ , gaussian functions  $M = 200$ , samples number  $N = 5000$ .

### 3.2 2-dimensional problem with coupled drift terms

Sombrero potential  $V$  is a well-known potential form that symmetry breaking is triggered in quantum mechanics. The gradient of the potential acts as the force and gives the drift term of the stochastic process as  $\mu = \nabla V$ . Figure 3 shows the sombrero potential  $V$  and its gradient  $\mu_1 = \partial_{x_1} V$  and  $\mu_2 = \partial_{x_2} V$  in the two dimensional space. The drift term induced by the Sombrero potential has the coupled terms in each dimension, i.e.,  $\mu_1$  and  $\mu_2$  are not independent. To illustrate the ability to reveal hidden stochastic dynamics with coupled drift terms, we apply the WCR method to the aggregate data generated by the 2-dimensional Brownian motion with the coupled drift term

$$\mu = -\nabla V = \begin{pmatrix} 10x_1 - 4x_1^3 - 4x_1x_2^2 \\ 10x_2 - 4x_2x_1^2 - 4x_2^3 \end{pmatrix}, \quad (33)$$

which is induced by the gradients of the Sombrero potential

$$V = -5\|\mathbf{x}\|^2 + \|\mathbf{x}\|^4 = -5(x_1^2 + x_2^2) + (x_1^2 + x_2^2)^2. \quad (34)$$

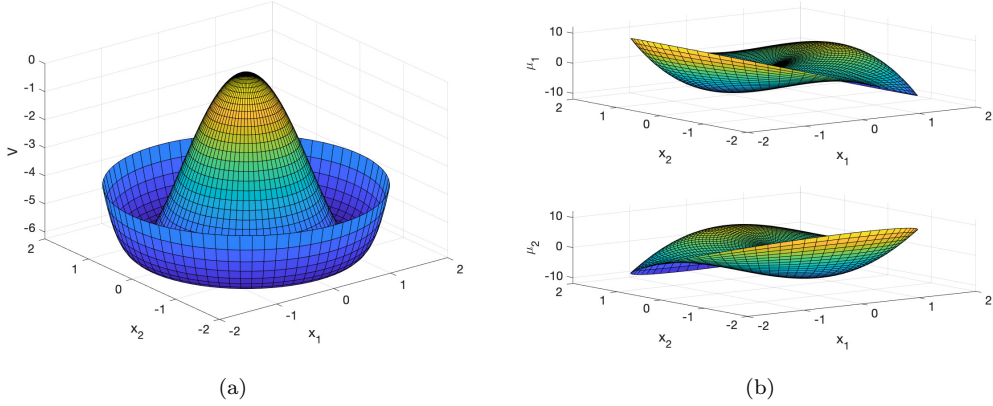


Figure 3: The 2-dimensional sombrero potential (a) and its derivatives (b) with respect to the spatial variables.

The true model decorated by the coupled drift (33) has the SDE form

$$d\mathbf{x} = \begin{pmatrix} c_{11}x_1^1 + c_{12}x_1^3 + c_{13}x_1x_2^2 \\ c_{21}x_2^2 + c_{22}x_1^2x_2 + c_{23}x_2^3 \end{pmatrix} dt + \begin{pmatrix} \sigma_1 & 0 \\ 0 & \sigma_2 \end{pmatrix} dW_t, \quad (35)$$

where  $c_{11} = c_{21} = 10$ ,  $c_{12} = c_{13} = c_{22} = c_{23} = -4$  corresponding to the coupled drift term (33) and  $\sigma_1 = \sigma_2 = 1$  for simplicity.

The raw data are generated by integrating the SDE from 40,000 initial samplings from the Gaussian distributions at  $t = 0$  to  $t = 15$  using the Euler-Maruyama method. Take  $N = 20,000$  samples out of the total 40,000 points in each snapshot and collect totally  $L = 151$  snapshots at  $t = 0, 0.1, \dots, 15$ , we have the aggregate data set  $\mathbb{X} = \{\mathbb{X}\}_{i=1}^L = \{\{\mathbf{x}_i^j\}_{j=1}^N\}_{i=1}^L$  for the experiment. In this subsection, we apply the WCR method to the data to reveal the true model and give a direct illustration of the performance of our method.

To reveal the hidden dynamics of the 2-dimensional stochastic process, 200 gaussian kernels are randomly sampled in the regime of the data, and the Milne method (12) is used to approximate the temporal derivatives. The elements of the unknown drift and coefficient term are approximated by the linear combinations of the forth-order complete polynomial basis

$$\Lambda = \{1, x_1, x_2, x_1^2, x_1x_2, x_2^2, x_1^3, x_1^2x_2, x_1x_2^2, x_2^3, x_1^4, x_1^3x_2, x_1^2x_2^2, x_1x_2^3, x_2^4\}, \quad (36)$$

with  $|\Lambda| = 15$ . For simplicity we denote the basis vector  $\mathbf{\Lambda} = (1, x_1, x_2, \dots, x_2^4)^T$  which is the vectorization of  $\Lambda$ . Note that the highest order of the drift term is three in the true model, but we have used a higher order term to approximate the unknown terms of both drift and diffusion terms. It follows that the unknown drift and diffusion terms are approximated by the following form

$$\boldsymbol{\mu} = \begin{pmatrix} \mu_1 \\ \mu_2 \end{pmatrix} = \begin{pmatrix} \boldsymbol{\zeta}_1^\mu \cdot \mathbf{\Lambda} \\ \boldsymbol{\zeta}_2^\mu \cdot \mathbf{\Lambda} \end{pmatrix}, \quad D = \begin{pmatrix} D_{11} & D_{12} \\ D_{21} & D_{22} \end{pmatrix} = \begin{pmatrix} \boldsymbol{\zeta}_{11}^D \cdot \mathbf{\Lambda} & \boldsymbol{\zeta}_{12}^D \cdot \mathbf{\Lambda} \\ \boldsymbol{\zeta}_{21}^D \cdot \mathbf{\Lambda} & \boldsymbol{\zeta}_{22}^D \cdot \mathbf{\Lambda} \end{pmatrix}, \quad (37)$$

where  $\boldsymbol{\zeta}_i^\mu \in \mathbb{R}^d$ ,  $\boldsymbol{\zeta}_{ij}^D \in \mathbb{R}^d$  are coefficient vectors with dimension  $d = |\Lambda| = 15$ . Thus for each drift term and each element of the diffusion matrix, we have 15 coefficients, making a total of 90 parameters to be revealed. By a sparse linear regression, instead of the 90 coefficients for a fourth-order complete

Parameter	$c_{11}$	$c_{12}$	$c_{13}$	$c_{21}$	$c_{22}$	$c_{23}$	$\sigma_1$	$\sigma_2$
True parameters	10	-4	-4	10	-4	-4	1	1
WCR	9.7823	-3.9032	-3.9364	9.8495	-3.9441	-3.9409	0.9881	1.0076

Table 5: The results of the 2-dimensional problem with Sombrebro potential. Reveal the unknown drift and diffusion terms with the expansion of the fourth-order complete polynomial basis. No redundant coefficients have been learned, with only 8 out of the 90 coefficients nonzero corresponding to the true model. The Max Relative Error of the nonzero coefficients is 2.42%.

polynomial basis, only eight coefficients corresponding to those in (35) are listed for simplicity, as the others are identified correctly as zero. All nonzero terms of the true model are not missed, and no redundant coefficients, which should be zeros, are not superfluous by the WCR method. The results are shown in Table 5. The Max Relative Error (MRE) is about 2.42% of the coefficients. The experiment is done on the Macbook pro within 21 seconds. The results in Table 5 illustrate the abilities of the WCR method for revealing hidden dynamics with coupled terms under high-order expansion.

### 3.3 Multi-dimensional problem

Many methods depending on the integration over space, always get stuck when the dimension of the data increases because of the exponential increase of the computational cost. Even under three or four dimensions, the integration is computationally expensive, despite the incapacity for higher dimensions such as 10d or 20d. In contrast, the WCR method takes a more subtle strategy to avoid the direct computation of the integral. Thanks to the weak form, the spatial derivatives of the probability function have been transferred to the test function, making the integral simply computed by the summation over the samples avoiding the curse of dimensionality. Hence WCR method can be naturally extended to the higher dimension other than one or two dimensions.

In this subsection, we take the same setup consistent with the 3d and 4d problems in [24] and show that the WCR method can achieve high accuracy within seconds. The true model is a d-dimensional extension of the SDE (29) with the form

$$dX_t^i = (X_t^i - (X_t^i)^3) dt + dW_t^i, \quad i = 1, 2, \dots, d, \quad (38)$$

where the drift term is  $\mu_i = x_i - x_i^3$  in the  $i$ -th dimension. The raw data are generated by the true model using the Euler-Mayaruma method. To get the aggregate data set, 100,000 samples each snapshot are taken and the snapshots at (i)  $t = 0.1, 0.3, 0.5, 0.7, 1$  (ii)  $t = 0.1, 0.2, 0.3, 0.5, 0.7, 0.9, 1$  are collected as the experimental data.

In the experiment, the unknown drift term in each dimension is approximated by

$$\hat{\mu}_i = \theta_0 + \theta_1 x_i + \theta_2 x_i^2 + \theta_3 x_i^3, \quad (39)$$

and the diffusion term approximated by a tunable parameter  $D_i$ ,  $i = 1, 2, \dots, d$ . 100 Gaussian kernels are sampled by the expectations using the LHS method with the default standard derivation where  $\gamma = 1$ . We list the Max Relative errors and the computational time in Table 6, and the results show that our WCR method achieves high accuracy in the 3d and 4d cases within seconds on the MacBook Pro.

	3D-(i)	3D-(ii)	4D-(i)	4D-(ii)
MRE	3.39%	1.86%	7.04%	3.18%
Time(s)	3.6	4.7	6.1	7.9

Table 6: The Max Relative Error of the learned coefficients and the computational time on the MacBook Pro of revealing the unknown 3d, 4d cubic polynomial problems. The aggregate data  $\mathbb{X}$  is composed of the time snapshots at (i)  $t = 0.1, 0.3, 0.5, 0.7, 0.9$  (ii)  $t = 0.1, 0.2, 0.3, 0.5, 0.7, 0.9, 1$  with 100,000 points in each snapshot. The unknown dynamics is approximated by the drift  $\hat{\mu}_i = \theta_0 + \theta_1 x_i + \theta_2 x_i^2 + \theta_3 x_i^3$  and diffusion  $D_i$  in each dimension with tunable parameters  $\theta_i$  and  $D_i$ ,  $i = 1, 2, \dots, d$ . Moreover, 100 gaussian kernels are sampled to give the composed linear system.

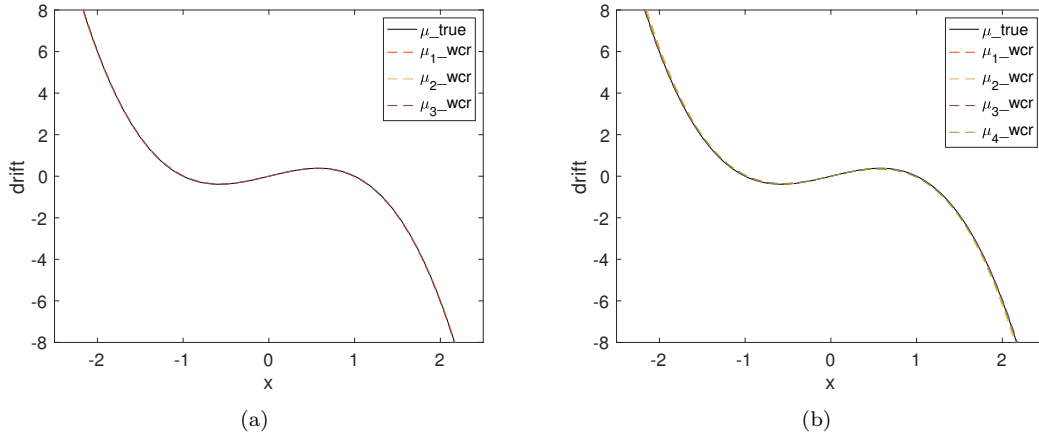


Figure 4: The learned drift terms of the 3d and 4d problems. Reveal the unknown drift and diffusion terms with 100,000 samples each snapshot at time  $t = 0.1, 0.3, 0.5, 0.7, 1$  of (a) 3-dimensional problem; (b) 4-dimensional problem, where the samples are generated by the given SDE with drift term  $\mu_{\text{true}} = x - x^3$  and diffusion term  $\sigma = 1$  in per dimension. The inference results are denoted by  $\mu_{\text{true}}$  and  $\mu_i_{\text{wcr}}$  for the  $i$ -th dimension.

### 3.4 High-dimensional problem

For three or four-dimensional data, the WCR method shows high accuracy in revealing the hidden stochastic dynamics. The higher dimensional problem, especially over ten-dimensional, brings more challenges to the modeling task because of the so-called curse of dimensionality. In this subsection, we will show that the WCR method can be applied to high-dimensional problems thanks to the Monte Carlo approximation of the weak form. We consider the ten and 20-dimensional aggregate data generated by the true model

$$dX_t^i = (X_t^i - (X_t^i)^3) dt + dW_t^i, \quad i = 1, 2, \dots, d, \quad (40)$$

with  $d = 10, 20$  using Euler-Maruyama method. Several time snapshots of the data at time  $t = 0, 0.1, 0.2, 0.3, \dots, 1$  are used as the experiment data.

In the experiment, the fourth order basis is used to approximate the drift term in each dimension as  $\mu_i = \theta_0 + \theta_1 x_i + \theta_2 x_i^2 + \theta_3 x_i^3$  and the diffusion term is approximated by a tunable parameter  $\sigma_i$ , making totally  $5d$  tunable parameters to be learned. The Milne method is used for the temporal derivatives. The different number of data samples in each snapshot and the Gaussian kernels are considered in the high-dimensional problem.

In the 10-dimensional problem, we consider the four cases for samples and kernels (a) 10,000 samples of  $X_t$  using 1000 Gaussian kernels; (b) 100,000 samples of  $X_t$  using 1000 Gaussian kernels; (c) 10,000 samples of  $X_t$  using 10,000 Gaussian kernels; (d) 100,000 samples of  $X_t$  using 10,000 Gaussian kernels. The four cases are the combinations of the 10,000 and 100,000 samples with 1000 and 10,000 Gaussian kernels. Figure 5 gives the display of the learned drift terms compared with the true model in each case. From the Figure, it is easy to check that the learned results get better when the number of the sample points and Gaussian kernels increases. Moreover, the Max Relative Error for the best result in case (d) achieves less than 7.8% within 20 minutes.

In the 20-dimensional case, we take 10,000 gaussian kernels and 100,000 samples of  $X_t$ . The experiment was completed within 47 minutes on the MacBook Pro, and the result is shown in Figure 6

### 3.5 Performance on data of different qualities

In real applications, the data obtained by various means usually contain many missing points and even flaws. The data may also be noisy, with sound signals deeply buried. These facts make analyzing and extracting valuable models from the data complicated and tricky. We have shown that WCR performs well with only several snapshots with non-equally spaced data in the one-dimensional case. In this subsection, we further investigate the performance of WCR on the data with different qualities, such as short and long time intervals, different numbers of samples in the snapshots, and noises.

The true model in this experiment has the following form

$$\begin{aligned} dx_1 &= -0.5x_1 dt + dW_t \\ dx_2 &= -0.7x_2 dt + dW_t \\ dx_3 &= -x_3 dt + dW_t, \end{aligned} \quad (41)$$

where the three dimensions are not coupled for simplicity and mainly focus on the data qualities. The raw data are generated by integrating the true model from  $t = 0$  to  $t = 10$ , and different kinds of snapshots are chosen as the aggregate data. Noise is added for the study of the noise effect.

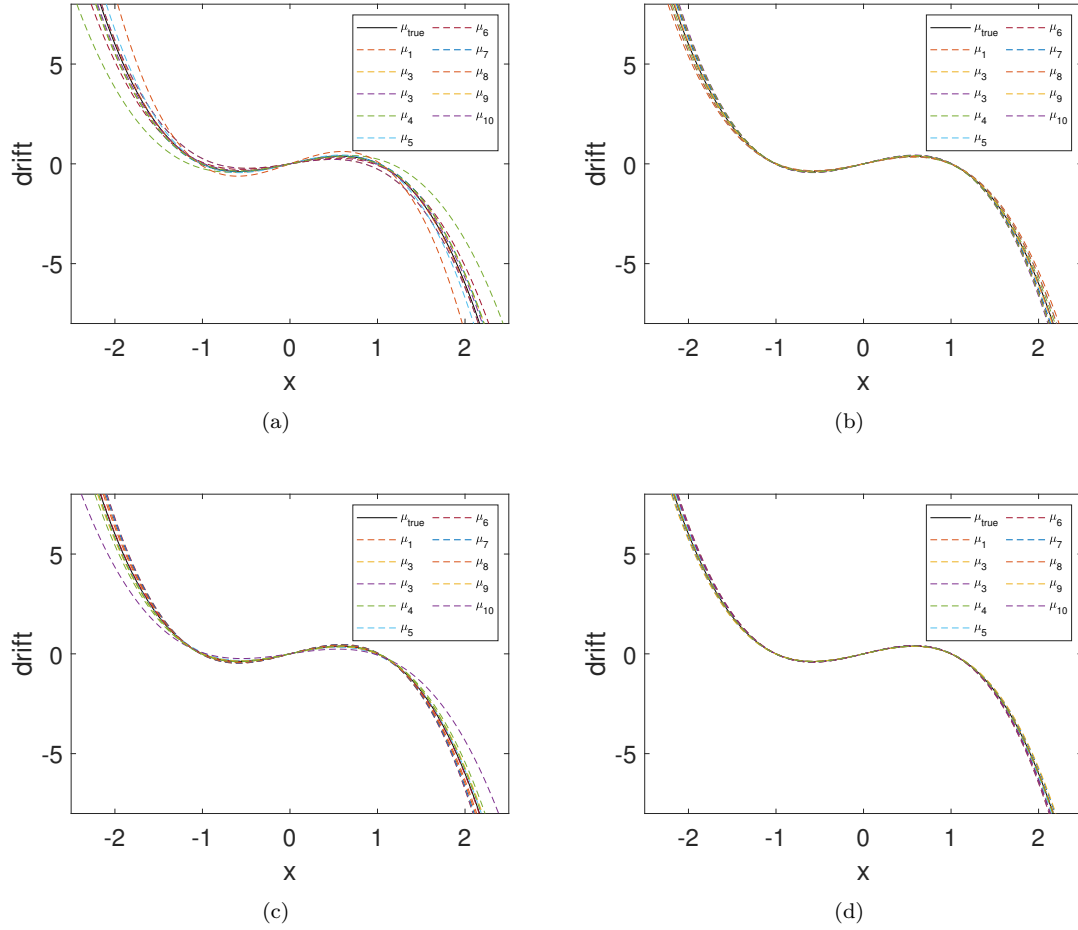


Figure 5: The results of 10d problems with the different number of samples per time snapshot and gaussian kernels. Reveal the unknown drift and diffusion terms with (a) 10,000 samples of  $X_t$  using 1000 gaussian kernels; (b) 100,000 samples of  $X_t$  using 1000 gaussian kernels; (c) 10,000 samples of  $X_t$  using 10,000 gaussian kernels; (d) 100,000 samples of  $X_t$  using 10,000 gaussian kernels at time snapshots  $t = 0, 0.1, 0.2, 0.3, 0.4, 0.5, 0.6, 0.7, 0.8, 0.9, 1$  of 10-dimensional problem, where the samples are generated by the given SDE with drift term  $\mu_{\text{true}} = x - x^3$  and diffusion term  $\sigma = 1$  in per dimension. The inference results are denoted by  $\mu_i$  for the learned drift in the  $i$ -th dimension.

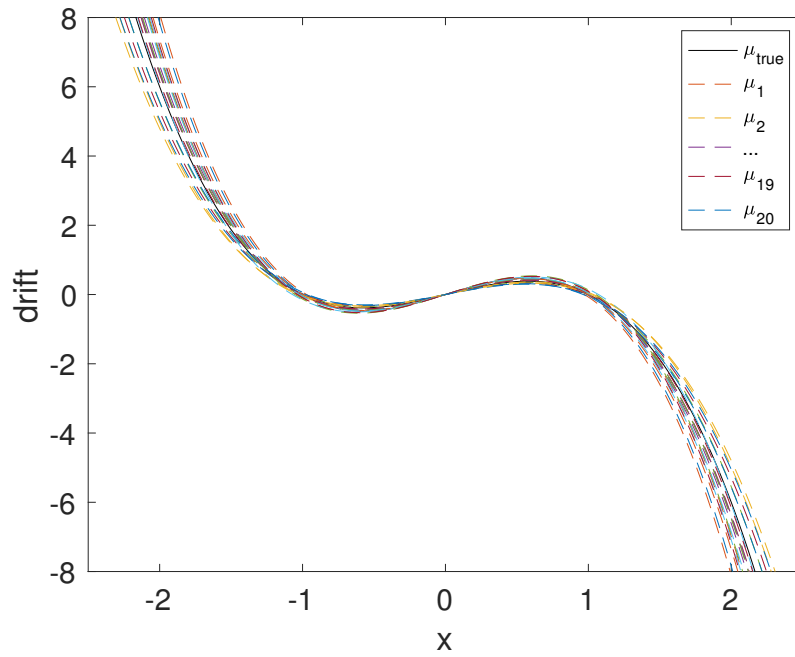


Figure 6: The results of 20-dimensional problems with 100,000 samples of  $X_t$  using 10,000 gaussian kernels at time  $t = 0, 0.1, 0.2, 0.3, 0.4, 0.5, 0.6, 0.7, 0.8, 0.9, 1$ , where the samples are generated by the given SDE with drift term  $\mu_{\text{true}} = x_i - x_i^3$  and diffusion term  $\sigma = 1$  in per dimension. The inference results are denoted as  $\mu_i$  for the  $i$ -th dimensional drift.

To reveal the hidden dynamics, the unknown drift term is expanded by the first order complete polynomials as

$$\text{drift} = \begin{pmatrix} \theta_{00} + \theta_{01}x_1 + \theta_{02}x_2 + \theta_{03}x_3 \\ \theta_{10} + \theta_{11}x_1 + \theta_{12}x_2 + \theta_{13}x_3 \\ \theta_{20} + \theta_{21}x_1 + \theta_{22}x_2 + \theta_{23}x_3 \end{pmatrix}, \quad (42)$$

and the diffusion matrix is approximated by a diagonal matrix  $D = \begin{pmatrix} \sigma_1 & & \\ & \sigma_2 & \\ & & \sigma_3 \end{pmatrix}$ , where  $[\theta_{ij}]$  and  $[\sigma_i]$  are tunable parameters to be revealed.

**Time interval and sample number.** We investigate in this part how the time interval and the sample number of the data affect the accuracy of the results in our WCR method. We consider four cases of the time interval  $\Delta t_1 = 0.1$ ,  $\Delta t_1 = 0.2$ ,  $\Delta t_1 = 0.5$  and  $\Delta t_1 = 1$  of the snapshots in the total interval  $[0, 10]$ . To be concise, the total number of the snapshots  $L = \frac{T}{\Delta t} + 1$ , where  $T = 10$ , and  $\Delta t$  is one of the time intervals. For example, we have  $L = 11$  snapshots in the case of  $\Delta t_4 = 1$ , with each snapshot being equally spaced with  $\Delta t_4 = 1$ . For the number of the samples in each snapshot, we also consider four cases with  $N_1 = 1000$ ,  $N_2 = 2000$ ,  $N_3 = 5000$ , and  $N_4 = 10,000$ . Thus we have totally tested  $4 \times 4 = 16$  cases to investigate the performance of WCR on the time interval and sample number of the data.

In all experiments, other setups are kept the same where 100 Gaussian functions with standard variance  $\gamma = 1$  are sampled as the test functions. Moreover, the trapezoidal rule is used for the temporal derivatives if  $\Delta t = 0.1, 0.2$  and the Milne method is used for the big time interval  $\Delta t = 0.5, 1$ . The Milne method with higher order accuracy is used in the big intervals to achieve better accuracy.

We summarize all the results in Figure 7. With only  $N = 1000$  samples and mild time interval  $\Delta t = 1$ , the maximum relative error can reach a good accuracy below 4%. Further, with the increasing number of samples in each snapshot and the decreasing time interval from  $\Delta t_4 = 1$  to  $\Delta t_1 = 0.1$ , from  $N_1 = 1000$  to  $N_2 = 10,000$ , the results generally get better. Moreover, all of the cases result in a low Max Relative Error, giving proof of the robustness of our method in relatively poor data quality.

**Noise.** In this part, we consider the performance of our WCR method on noisy data. The raw data are obtained by the same procedure as the above, and the random noise is added with the noise level  $\delta$

$$\hat{\mathbf{x}}_i^j = \mathbf{x}_i^j + \delta \mathcal{U}_i^j \mathbf{x}_i^j,$$

where  $\mathcal{U}_i^j$  is a uniform random variable in  $[0, 1]$ . Here the data with 10,000 samples in each snapshot are used, and two kinds of time intervals are chosen to show the robustness of our methods on the noise.

The results are listed in Table 7, and the Max Relative Error reaches around 5% with the white noise level  $\delta = 10\%$  for both two cases. Further, when we dive into the detail of the accuracy for drift and diffusion terms, respectively, adding noise to the data did not change the accuracy of the drift term much, unlike the diffusion term.

## 4 Conclusion

In this work, leveraging the weak form of the Fokker-Planck equation and the collocations of the Gaussian kernels, we proposed a framework called the Weak Collocation Regression method (WCR) to fast reveal the hidden stochastic dynamics from high-dimensional aggregate data. The lack of

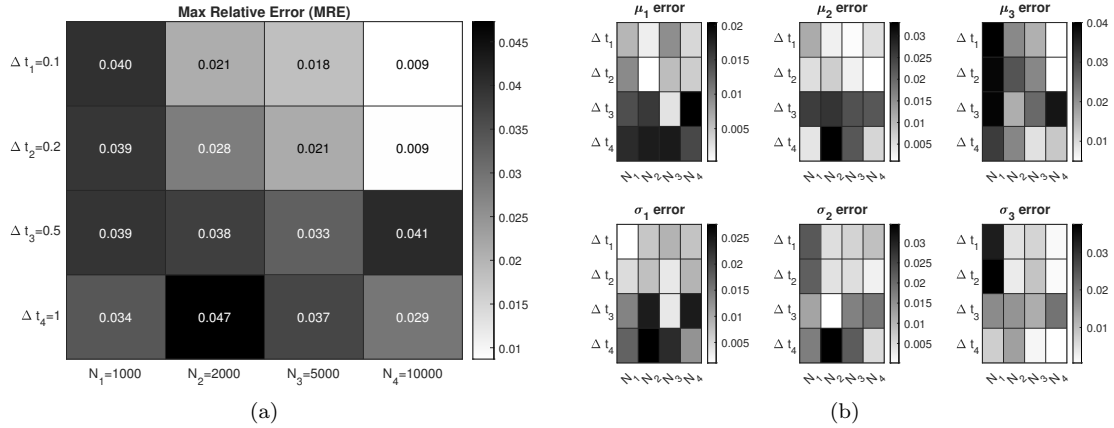


Figure 7: The heat map of the errors of the drift coefficients and diffusion for the 3-dimensional stochastic process in  $T = [0, 10]$  with different trajectory samples  $N_1 = 1000, N_2 = 2000, N_3 = 5000, N_4 = 10,000$  and different time interval  $\Delta t_1 = 0.1, \Delta t_2 = 0.2, \Delta t_3 = 0.5,$  and  $\Delta t_4 = 1$ . The true governing stochastic equation reads  $dx_1 = -0.5x_1dt + dW_1, dx_2 = -0.7x_2dt + dW_2,$  and  $dx_3 = -x_3dt + dW_3,$  where the coefficients of  $\mu_1, \mu_2,$  and  $\mu_3$  are  $-0.5, -0.7$  and  $-1,$  and the diffusions  $\sigma_1 = \sigma_2 = \sigma_3 = 1$ . (a) shows the max relative error of the coefficients for  $N_i$  and  $\Delta t_j$ ; (b) shows the relative error of per coefficient for  $N_i$  and  $\Delta t_j$  with  $i, j = 1, 2, 3, 4$ .

	$\Delta t = 0.1, \delta = 0\%$	$\Delta t = 0.1, \delta = 10\%$	$\Delta t = 0.5, \delta = 0\%$	$\Delta t = 0.5, \delta = 10\%$
MRE	1.87%	5.76%	1.46%	6.01%
MRE in drift	1.87%	1.75%	1.46%	1.04%
MRE in diffusion	0.72%	5.76%	0.77%	6.01%

Table 7: The results of a three-dimensional linear problem with different time snapshots and noise. Reveal the unknown drift and diffusion terms with  $\Delta t = 0.1, 0.5$  and  $\delta = 0\%, 10\%$ , where 10,000 samples each snapshot are generated by the given SDE with drift term  $\mu(x, y, z) = [-0.5x, -0.7y, -z]^T$  and diffusion term  $\sigma = I_{3 \times 3}$ .

trajectory information makes aggregate data (unpaired data) more difficult to reveal the hidden dynamics. However, the data distribution follows the Fokker-Planck equation under some assumptions, such as the Brownian motion. By transferring the spatial derivatives to the test function in the weak form of the Fokker-Planck equation, we have an integral form of the density function with derivatives of the test functions. Thus the integral form can be easily approximated by summing the derivatives of the test functions over the samples. Using collocations of the Gaussian functions as the test functions and the dictionary representation of the unknown terms, we build an extensive linear system. Linear regression and sparse identification lead to unknown terms, thus revealing the hidden dynamics.

Our experiments show that WCR is numerically efficient, taking only 0.02s on the Macbook Pro for the 1-dimensional problem with comparable accuracy and seconds for multi-dimensional problems. With the LMMs of variable step size, WCR achieves good accuracy in the non-equally spaced time data. Approximating the integral form using the summations over samples makes the WCR method naturally relieve the curse of dimensionality. Furthermore, the extra computational cost is required on the collocations of the kernels but does not exponentially increase with dimension. WCR still works well when the dimension increases to 20 within an hour on MacBook Pro. The variable-dependent diffusion problem and coupled drift terms usually bring more difficulties, but the WCR method exhibits high accuracy in these complex problems. Furthermore, for the data with noise, the WCR method also obtains a stable performance when adding the white noise. With different time intervals and samples, WCR shows its robustness without losing too much accuracy when the data quality worsens.

Despite the advantages mentioned above, the Weak Collocation Regression method still has some limitations for investigation in future work. Our approach slows down for the ultimately high-dimensional problems such as 100 dimensions since more Gaussian kernel collocations are needed, requiring high computational costs. More effective sampling schemes, such as active learning for the collocation of the Gaussian kernels, are necessary to reduce the computational cost. Neural networks might be another choice for the test function with a min-max optimization for reducing the cost. Further, the drift and diffusion terms may be approximated by neural networks to give a good approximation in the high dimension. Further discussion about the convergence results and a general form besides the Brownian motion is needed but left for future work.

## Acknowledgements

This work was supported by the National Key R&D Program of China (Grant No. 2021YFA0719200) and the National Science Foundation of China (Grant No. 12071244). The authors would like to thank the helpful discussions from Dr. Liu Hong.

## References

- [1] Roger Temam. *Navier-Stokes equations: theory and numerical analysis*, volume 343. American Mathematical Soc., 2001.
- [2] Leslie E Ballentine. *Quantum mechanics: a modern development*. World Scientific Publishing Company, 2014.
- [3] Peter Klein. Pricing black-scholes options with correlated credit risk. *Journal of Banking & Finance*, 20(7):1211–1229, 1996.

- [4] Daniel Dufresne. The integral of geometric brownian motion. *Advances in Applied Probability*, 33(1):223–241, 2001.
- [5] Ian Goodfellow, Yoshua Bengio, and Aaron Courville. *Deep learning*. MIT press, 2016.
- [6] Maziar Raissi, Paris Perdikaris, and George E Karniadakis. Physics-informed neural networks: A deep learning framework for solving forward and inverse problems involving nonlinear partial differential equations. *Journal of Computational Physics*, 378:686–707, 2019.
- [7] Steven L Brunton, Joshua L Proctor, and J Nathan Kutz. Discovering governing equations from data by sparse identification of nonlinear dynamical systems. *Proceedings of the National Academy of Sciences*, 113(15):3932–3937
- [8] Pipi Hu, Wuyue Yang, Yi Zhu, and Liu Hong. Revealing hidden dynamics from time-series data by odenet. *Journal of Computational Physics*, 461:111203, 2022.
- [9] Zichao Long, Yiping Lu, Xianzhong Ma, and Bin Dong. Pde-net: Learning pdes from data. In *International Conference on Machine Learning*, pages 3208–3216, 2018.
- [10] Zichao Long, Yiping Lu, and Bin Dong. Pde-net 2.0: Learning pdes from data with a numeric-symbolic hybrid deep network. *Journal of Computational Physics*, 399:108925, 2019.
- [11] Gert-Jan Both, Subham Choudhury, Pierre Sens, and Remy Kusters. Deepmod: Deep learning for model discovery in noisy data. *Journal of Computational Physics*, 428:109985, 2021.
- [12] Zhao Chen, Yang Liu, and Hao Sun. Physics-informed learning of governing equations from scarce data. *Nature communications*, 12(1):1–13, 2021.
- [13] Guochang Lin, Pipi Hu, Fukai Chen, Xiang Chen, Junqing Chen, Jun Wang, and Zuoqiang Shi. Binet: Learning to solve partial differential equations with boundary integral networks. *arXiv preprint arXiv:2110.00352*, 2021.
- [14] Qin Lou, Xuhui Meng, and George Em Karniadakis. Physics-informed neural networks for solving forward and inverse flow problems via the boltzmann-bgk formulation. *Journal of Computational Physics*, 447:110676, 2021.
- [15] Lu Lu, Pengzhan Jin, and George Em Karniadakis. Deeponet: Learning nonlinear operators for identifying differential equations based on the universal approximation theorem of operators. *arXiv preprint arXiv:1910.03193*, 2019.
- [16] Shaojun Ma, Shu Liu, Hongyuan Zha, and Haomin Zhou. Learning stochastic behaviour from aggregate data. In *International Conference on Machine Learning*, pages 7258–7267. PMLR, 2021.
- [17] Liu Yang, Constantinos Daskalakis, and George E Karniadakis. Generative ensemble regression: Learning particle dynamics from observations of ensembles with physics-informed deep generative models. *SIAM Journal on Scientific Computing*, 44(1):B80–B99, 2022.
- [18] Samuel Greydanus, Misko Dzamba, and Jason Yosinski. Hamiltonian neural networks. *Advances in Neural Information Processing Systems*, 32, 2019.
- [19] Daniel Alshamaa, Aly Chkeir, Farah Mourad-Chehade, and Paul Honeine. A hidden markov model for indoor trajectory tracking of elderly people. In *2019 IEEE Sensors Applications Symposium (SAS)*, pages 1–6. IEEE, 2019.

- [20] Maryam Baradaran Khalkhali, Abedin Vahedian, and Hadi Sadoghi Yazdi. Vehicle tracking with kalman filter using online situation assessment. *Robotics and Autonomous Systems*, 131:103596, 2020.
- [21] Nuno Pessanha Santos, Victor Lobo, and Alexandre Bernardino. Unmanned aerial vehicle tracking using a particle filter based approach. In *2019 IEEE Underwater Technology (UT)*, pages 1–10. IEEE, 2019.
- [22] Yongkun Fang, Chao Wang, Wen Yao, Xijun Zhao, Huijing Zhao, and Hongbin Zha. On-road vehicle tracking using part-based particle filter. *IEEE transactions on intelligent transportation systems*, 20(12):4538–4552, 2019.
- [23] Qiang Du, Yiqi Gu, Haizhao Yang, and Chao Zhou. The discovery of dynamics via linear multistep methods and deep learning: Error estimation. *SIAM Journal on Numerical Analysis*, 60(4):2014–2045, 2022.
- [24] Xiaoli Chen, Liu Yang, Jinqiao Duan, and George Em Karniadakis. Solving inverse stochastic problems from discrete particle observations using the fokker-planck equation and physics-informed neural networks. *SIAM Journal on Scientific Computing*, 43(3):B811–B830, 2021.
- [25] Martin Arjovsky, Soumith Chintala, and Léon Bottou. Wasserstein generative adversarial networks. In *International conference on machine learning*, pages 214–223. PMLR, 2017.
- [26] Richard E Bellman. Adaptive control processes. In *Adaptive Control Processes*. Princeton university press, 2015.
- [27] Hannes Risken. Fokker-planck equation. In *The Fokker-Planck Equation*, pages 63–95. Springer, 1996.
- [28] Lawrence C Evans. *Partial differential equations*, volume 19. American Mathematical Soc., 2010.
- [29] Yaohua Zang, Gang Bao, Xiaojing Ye, and Haomin Zhou. Weak adversarial networks for high-dimensional partial differential equations. *Journal of Computational Physics*, 411:109409, 2020.
- [30] Gang Bao, Xiaojing Ye, Yaohua Zang, and Haomin Zhou. Numerical solution of inverse problems by weak adversarial networks. *Inverse Problems*, 36(11):115003, 2020.
- [31] Samuel H Rudy, Steven L Brunton, Joshua L Proctor, and J Nathan Kutz. Data-driven discovery of partial differential equations. *Science Advances*, 3(4):e1602614, 2017.
- [32] Herman Heine Goldstine. *A History of Numerical Analysis from the 16th through the 19th Century*, volume 2. Springer Science & Business Media, 2012.
- [33] Kendall Atkinson, Weimin Han, and David E Stewart. *Numerical solution of ordinary differential equations*, volume 108. John Wiley & Sons, 2011.
- [34] Maziar Raissi, Paris Perdikaris, and George Em Karniadakis. Multistep neural networks for data-driven discovery of nonlinear dynamical systems. *arXiv preprint arXiv:1801.01236*, 2018.
- [35] Rachael T Keller and Qiang Du. Discovery of dynamics using linear multistep methods. *SIAM Journal on Numerical Analysis*, 59(1):429–455, 2021.

- [36] E Hairer SP Norsett and G Wanner. Solving ordinary differential equations i: Nonsti problems, 1987.
- [37] Michael Stein. Large sample properties of simulations using latin hypercube sampling. *Technometrics*, 29(2):143–151, 1987.
- [38] Bernt Oksendal. *Stochastic differential equations: an introduction with applications*. Springer Science & Business Media, 2013.
- [39] Ian Knowles and Robert J Renka. Methods for numerical differentiation of noisy data. *Electronic Journal of Differential Equations*, 21:235–246, 2014.

## Appendix

### A Method to compute temporal derivative

The right-hand side of equation (9) can be directly modified using the data set  $\mathbb{X}$ . However, the left-hand side should be carefully considered because of the temporal derivatives. There are several ways to handle the temporal derivatives of  $y(\mathbb{X}_t)$  in the discrete-time snapshots, where the most direct way is by the numerical scheme of the differentiation, e.g., Euler’s scheme or other schemes with high order. However, due to the high noise signal level of the data in the tasks of revealing stochastic dynamics, these schemes may encounter failure because of the data glitch. One practical solution is to use the schemes considering the smoothness. For example, Tikhonov differentiation [39] given by

$$\hat{y}' = (A^T A + \lambda M^T M)^{-1} A^T y, \quad (43)$$

where  $\hat{y}'$  is the approximation of the discrete form of  $y'(t)$ ,  $\lambda$  is a Tikhonov regularization,  $A$  and  $M$  come from the approximations to the integral and the derivatives. Tikhonov differentiation approximates the derivatives by the closeness of the integral with the balance of the smoothness

$$\hat{y}'(t) = \operatorname{argmin}_g \left\| \int_{t_0}^t g(s) ds - (y(t) - y(t_0)) \right\|_2^2 + \lambda \left\| \frac{dg}{dt} \right\|_2^2. \quad (44)$$

Approximate the integral and the derivatives. One obtains the discrete form

$$\hat{y}' = \operatorname{argmin}_g \|Ag - (y - y_0)\|_2^2 + \lambda \|Mg\|_2^2, \quad (45)$$

where  $A$  is a trapezoidal approximation to the integral and  $M$  is a finite difference approximation to the derivative.

Besides, the Adams-Moulton methods we used in this work is

$$\left\{ \begin{array}{l} y_n - y_{n-1} = hf_n \\ y_{n+1} - y_n = \frac{h}{2} (f_{n+1} + f_n) \\ y_{n+2} - y_{n+1} = h \left( \frac{5}{12} f_{n+2} + \frac{8}{12} f_{n+1} - \frac{1}{12} f_n \right) \\ y_{n+3} - y_{n+2} = h \left( \frac{9}{24} f_{n+3} + \frac{19}{24} f_{n+2} - \frac{5}{24} f_{n+1} + \frac{1}{24} f_n \right) \\ y_{n+4} - y_{n+3} = h \left( \frac{251}{720} f_{n+4} + \frac{646}{720} f_{n+3} - \frac{264}{720} f_{n+2} + \frac{106}{720} f_{n+1} - \frac{19}{720} f_n \right) \end{array} \right. \quad (46)$$

## B Discussion of the error

For a number of reasons, the Weak Collocation Regression method has a series of errors. It is necessary to find out the source of the error to improve the accuracy of our method. In general, the error of our method mainly comes from the following aspects:

1. The observation data of SDE

$$dX_t = \mu dt + \sigma dW_t. \quad (47)$$

Our experiment is inaccurate since the numerical error is contained in the discretization scheme in the data generating process. In this research, we use the Euler-Maruyama method to discrete the time  $[0, T]$  with interval  $\delta t$ , whose local truncation error is  $O(\delta t^2)$ . In our numerical experiments  $\delta t = 0.001$  or  $\delta t = 0.0001$  so the observation data error here becomes  $10^{-6}$  or  $10^{-8}$ . The initial distribution of SDE also matters a lot because it determines whether the SDE fully evolves within a specified time  $[0, T]$ .

2. Inaccurate observation generates a random error in the measurement process, which affects the identification of the drift and diffusion terms by introducing an error in assembling matrix  $A$  and vector  $b$ . For most nature dynamics, the observation data is due to the restriction of the experimental measurement and the measurement instrument. In this research, we show the robustness of our methods by adding white noise to observation data. The result shows the high insensitivity of our methods to noise. We can introduce the adaptive regularization parameter adjustment with respect to the noise level in the sparse regression process in the traditional Inverse Problem way for further improvement.
3. There exists error in computing the integration or expectation, such as  $\int_{\Omega} p(x, t) \boldsymbol{\mu}(\mathbf{x}) \cdot \nabla \psi(\mathbf{x}) dx$  or  $\mathbb{E}_{\mathbf{x} \sim p(\mathbf{x}, t)}[\boldsymbol{\mu}(\mathbf{x}) \cdot \nabla \psi(\mathbf{x})]$ . In this research, we use the Monte Carlo method to compute the integration, whose convergence error in probability is  $O(1/\sqrt{N})$ :

$$\lim_{N \rightarrow +\infty} \mathbb{P}\{|I_N - \int_{\Omega} g(x) dx| < \frac{\varepsilon \text{var}(g(x))}{\sqrt{N}}\} = \frac{1}{\sqrt{2\pi}} \int_{-\varepsilon}^{\varepsilon} e^{-\frac{t^2}{2}} dt \quad (48)$$

where  $N$  is the sample number, and  $I_N$  is the average of integrand among  $N$  samples. We can find that the error here plays a decisive role in our experimental results.

4. The Linear Multistep Methods to deal with the temporal derivative also produces an error. Given data of discrete time snapshots, the LMM provides only an approximation of their temporal derivative with residual errors. Some analyses and results already exist. Concerning the local truncated error, the M-step Adams-Moulton methods have an order of error  $M+1$ , while the M-step BDF has an error of order  $M$ . Moreover, the M-step BDF scheme and 0-step Adams-Moulton method are stable, while 1 step Adams-Moulton method is marginally stable. Hence the Adams methods of trapezoidal rule and BDF2 are both convergent. For the most rigorous conception and theorem, we refer to [23, 35].
5. After building linear systems, there exists an error in solving the parameter in the drift and diffusion term. In this research, we use linear regression with regularization to compute  $A\theta = y$ . If matrix  $A, b$  is accurate enough, then  $\theta$  is also accurate for the equation is over-determined. While the above three errors are objective, solving  $A\theta = y$  also produces an error that is related to the conditional number of  $A$ .